Al-Qadisiyah Journal of Pure Science
ISSN(Printed): 1997-2490 ISSN(Online): 2411-3514
DOI: 10.29350/jops
Al-Qadisiyah Journal of Pure Science

Synthesis and characterization of Pd(II) complexes with new Azo dapsone ligand and their Anticancer Studies with Biological Activity

Gufran Muhammed Salim 1 Haider M.Hessoon [1*]

Department of Chemistry, College of Science, University of Al-Qadisiyah, Al- Diwaniyah, Iraq

Corresponding author, emailsi.chem.mas.22.20@qu.edu.iq

Corresponding author, email haider19737654@gmail.com

ABSTRACT

In this experimental investigation, a novel ligand, SPD-DMN, derived from Dapsone and 3-methyl-4-nitrophenol, was synthesized and thoroughly characterized. Its pd(II) complex was also prepared and studied. The study confirmed the molecular weights of both compounds using mass spectrometry. The ^{1}H-NMR spectra indicated coordination events and proton loss in the complex. Infrared spectra showed coordination events related to the azo group. UV-Visible spectroscopy revealed electronic transitions, and X-ray diffraction analysis indicated nanoscale characteristics. However, the ligand's impact on liver cancer and normal cells demonstrated a lack of selectivity. Furthermore, both SPD-DMN and thepd (II) complex displayed moderate antioxidant potential when compared to ascorbic acid. Future research is essential to enhance selectivity and optimize antioxidant properties for potential therapeutic applications.

Keywords: pd(II)complex , Antioxidant properties, ,Bisazo ligand, Dapsone .

INTRODUCTION

In this particular experimental inquiry, a new ligand, known as SPD-DMN, which is a product of Dapsone and was synthesized and meticulously characterized. The corresponding pd(II) coordination compound was also synthesized and examined. The 1H-NMR spectra revealed instances of coordination and proton depletion within the coordination complex. Infrared spectra exhibited coordination phenomena associated with the azo functional group. Analysis via UV-Visible spectroscopy unveiled electronic transitions, while X-ray diffraction analysis indicated characteristics at the nanoscale level. Nonetheless. Additionally, both SPD-DMN and the pd(II) coordination complex showcased a moderate level of antioxidant activity in comparison to ascorbic acid. Subsequent research endeavors are imperative to refine specificity and optimize antioxidant attributes for potential therapeutic purposes.Cancer remains a formidable global health challenge(1), necessitating continual exploration of novel therapeutic agents with enhanced selectivity and reduced side effects. In this pursuit, the field of coordination chemistry has played a pivotal role by offering a diverse array of potential anticancer agents(2)–(4). Among the myriad of coordination compounds, bisazo ligands have garnered considerable attention due to their structural versatility and potential therapeutic applications(5), (6). In particular, the synthesis and characterization of bisazo ligands derived from 4,4'-Diaminodiphenyl sulfone (Dapsone) have opened new avenues in the search for effective anticancer agents(7), (8). This research embarks on a comprehensive investigation into the synthesis, characterization, and evaluation of the antioxidant and anticancer activities of a novel Dapsone-derived bisazo ligand, herein referred to as SPD-DMN, and its pd(II) complex.

SPD-DMN emerges as a unique ligand, showcasing intriguing properties that are poised to revolutionize the realm of coordination chemistry. The meticulous synthesis process leads to the formation of a orang powder characterized by an impressive yield and a notable melting point of 93.5°C. This ligand exhibits solubility in a range of solvents, presenting promising attributes for various applications. .

Beyond the structural intricacies, this research delves into the biological activities of SPD-DMN, addressing both its antioxidant potential and its capacity to combat breast cancer cells. Antioxidants have gained recognition for their role in mitigating oxidative stress and reducing the risk of various diseases, including cancer(9), (10). Therefore, the evaluation of SPD-DMN antioxidant activity is a crucial facet of this study. Additionally, the investigation extends to assessing the impact of SPD-DMN on breast cancer cells (HEPG2), providing critical insights into its selectivity and potential as an anticancer agent.

The findings of this research promise to contribute significantly to the fields of coordination chemistry and cancer therapeutics. By elucidating the synthesis, structure, and biological activities of SPD-DMN and its pd(II) complex, this study paves the way for the development of innovative and selective anticancer agents with the potential to enhance patient outcomes and reduce the burden of cancer worldwide..

EXPERIMENTAL SECTION

Materials

4,4′-Diaminodiphenyl(Dapsone) (FERAK, 99%), Sodium nitrite , (Thomas baker ,98%) , Sodium hydroxide (LOBA , 98%) , palladium(II) chloride (B.D.H, 98%) 3-methyl-4-nitrophenol (CDH, 99%) Hydrochloric acid (CGH, 38%), Dimethyl sulfoxide (LOBA, 99%)

Instrumentation

Shimadzu FT-IR 8400S Spectrophotometer, Uv- 1650 PC UV-Visible Spectrophotometer, Sturat digital melting Point / SMP3, Bruker500 MHZ300, Philips X'Pert Pro diffractometer

Procedure

preparation of Ligand (SPD-DMN)

In this synthetic procedure, 1.24 grams (0.005 moles) of 4,4'-Diaminodiphenyl sulfone were solubilized in a solution composed of 5 ml of 37% hydrochloric acid and 40 ml of distilled water, and the solution was meticulously cooled to a temperature of 5-0°C,

as depicted in the schematic representation. Subsequently, a solution containing 0.7 grams (1 mole) of sodium nitrite, dissolved in 25 ml of distilled water, was meticulously introduced drop by drop while maintaining continuous agitation, with stringent temperature control not to exceed 5°C, as clearly indicated in the graphical representation. Following this step, the solution was allowed to rest for a period of 15 minutes to ensure the completion of the diazotization process.Finally, the diazonium solution was introduced dropwise with constant agitation into a solution comprising 1.53 grams (0.01 mole) of 3-methyl-4nitrophenol, previously dissolved in a mixture consisting of 17 ml of 10% sodium hydroxide (NaOH) and 30 ml of ethanol, as meticulously illustrated in the scheme1 .

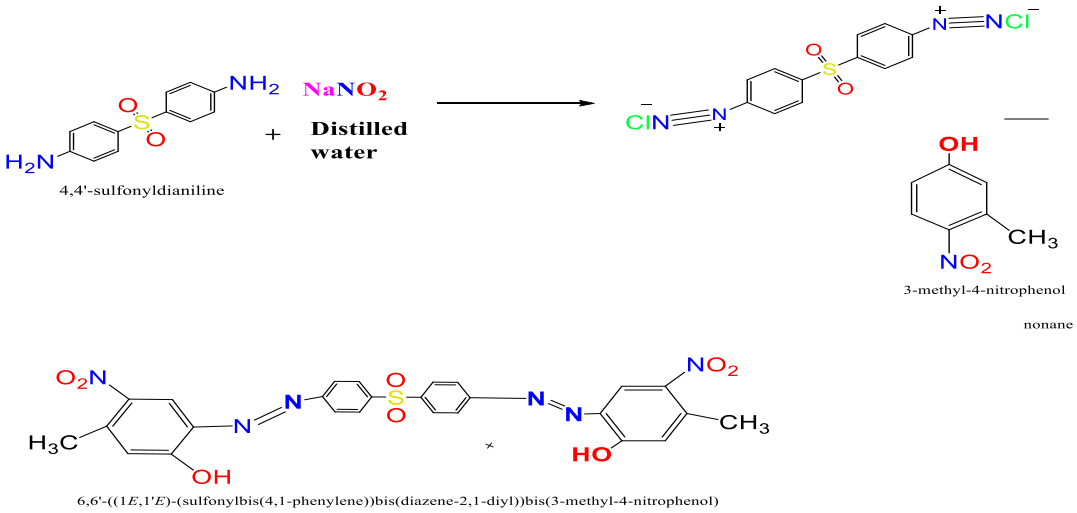

Scheme 1 Preparation steps of SPD-DMN ligand of bisazo based on Dapsone

Synthesis of pd(II) Complex

The complex (pdL2) was synthesized in a 2:1 molar ratio (ligand: metal) by dissolving 0.34 grams (0.001 mole) of palladium chloride(II) in (15 ml) of ammonium acetate solution and separately dissolving 0.57 grams (0.001 mole) of the ligand in (10 ml) of absolute ethanol. The mixture was refluxed for 60 minutes, resulting in the formation of a dark brown precipitate upon cooling. This precipitate was filtered, air-dried, and subsequently recrystallized from absolute ethanol to obtain the complex in its pure form.

RESULTS AND DISCUSSION

The resulting ligand, identified as 6,6'-((sulfonylbis(4,1-phenylene))bis(diazene-2,1diyl))bis(3-methyl-4-nitrophenol) (SPD-DMN), was acquired an 80% yield and a melting point of 93.5°C., the ligand displayed insolubility in water but complete solubility in various solvents such as dimethyl sulfoxide, dimethylformamide, and acetone.The synthesis process involved the reaction of pd(II) with SPD-DMN ligand in ethanol under reflux conditions, leading to the formation of a high-yield pd(II) complex distinguished by its dark brown colour and a melting point of 223°C.

1H Nuclear Magnetic Resonance (NMR) Spectroscopy

The pd (II) complex and the SPD-DMN ligand underwent a thorough 1H-NMR spectra analysis using DMSO-d6 as the solvent and TMS as the standard reference. The purpose of this analytical technique was to investigate possible coordination behaviors and structural changes.When comparing the 1H-NMR spectra of the pd(II) complex to that of the SPD-DMN ligand, noticeable shifts and changes in peak intensities were observed. The fact that the distinctive (OH) group peak was absent, indicating its role in coordination activities, was especially notable. This coordination event was accompanied by the loss of protons, ultimately culminating in the formation of the investigated complex

Table 1 HNMR Analysis of SPD-DMN and [pd2(SPD-DMN)$(H_2O)_4$] Complex: Proton Positions and Chemical Shifts (ppm)

Proton Position	SPD-DMN		Proton Position	[pd2(SPD-DMN)$CL_2(H_2O)_2$]	
	Chemical Shift (δ)	Signal Type		Chemical Shift (δ)	Signal Type
26,28	7.22ppm	Singlet	----------	----------	----------
32,33	11.44 ppm	Singlet			
6,10,11,15	7.60 ppm	Doublet	15, 5	8.21 ppm	Doublet
7,9,12,14	7.61 ppm	Doublet	11, 9	8.01 ppm	Doublet
22,31	7.59 ppm	Singlet	6 , 14	7.44 ppm	Doublet
34,35	7.95 ppm	Singlet	8, 12	7.22 ppm	Doublet

5 , 15	7.92 ppm	Singlet	19, 30	6.66 ppm	Singlet
24, 35	7.71 ppm	Singlet	21, 32	6.24 ppm	Doublet
H2O	3.35 ppm	Singlet	26, 37	2.62 ppm	Singlet
DMSO-d6	2.56 ppm	Singlet	25, 36	2.22 ppm	Singlet
			DMSO-d6	2.52 ppm	Singlet

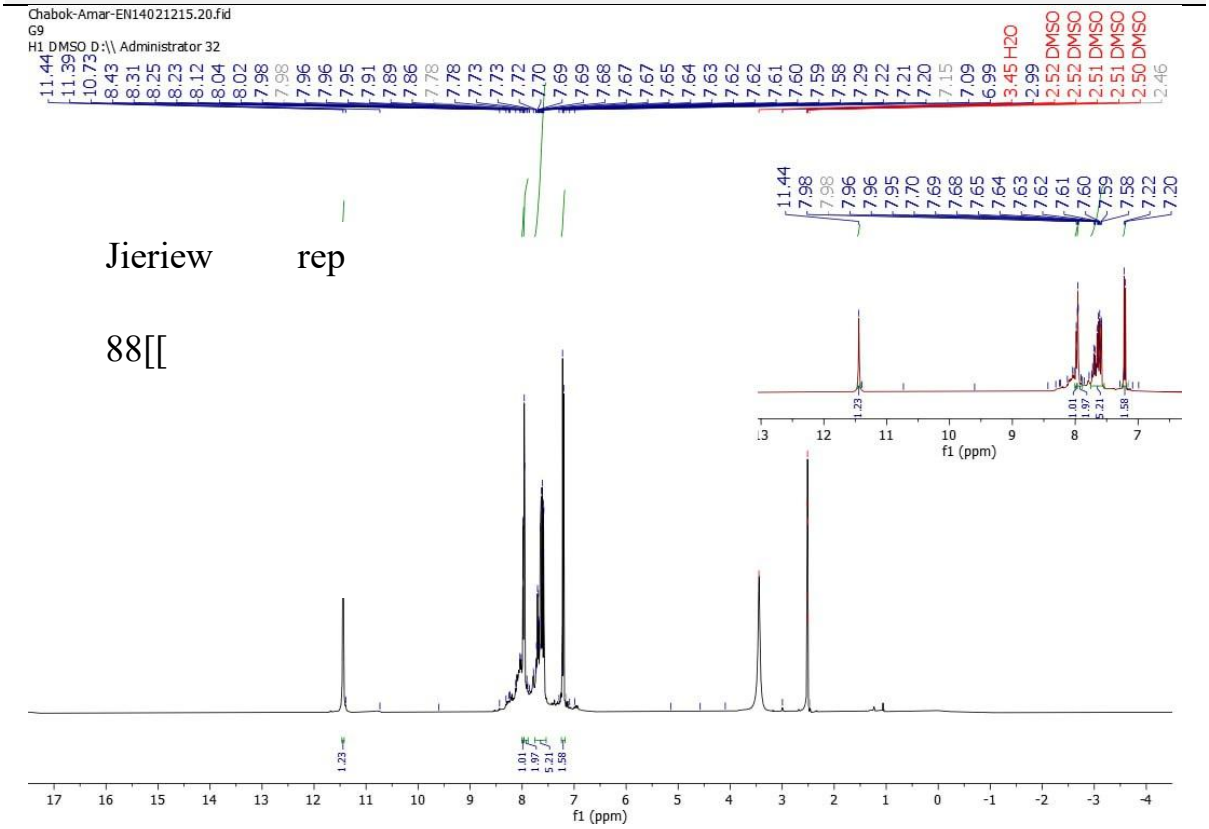

Figure 2 1HNMR spectrum of SPD-DMN ligand in DMSO d6 solvent

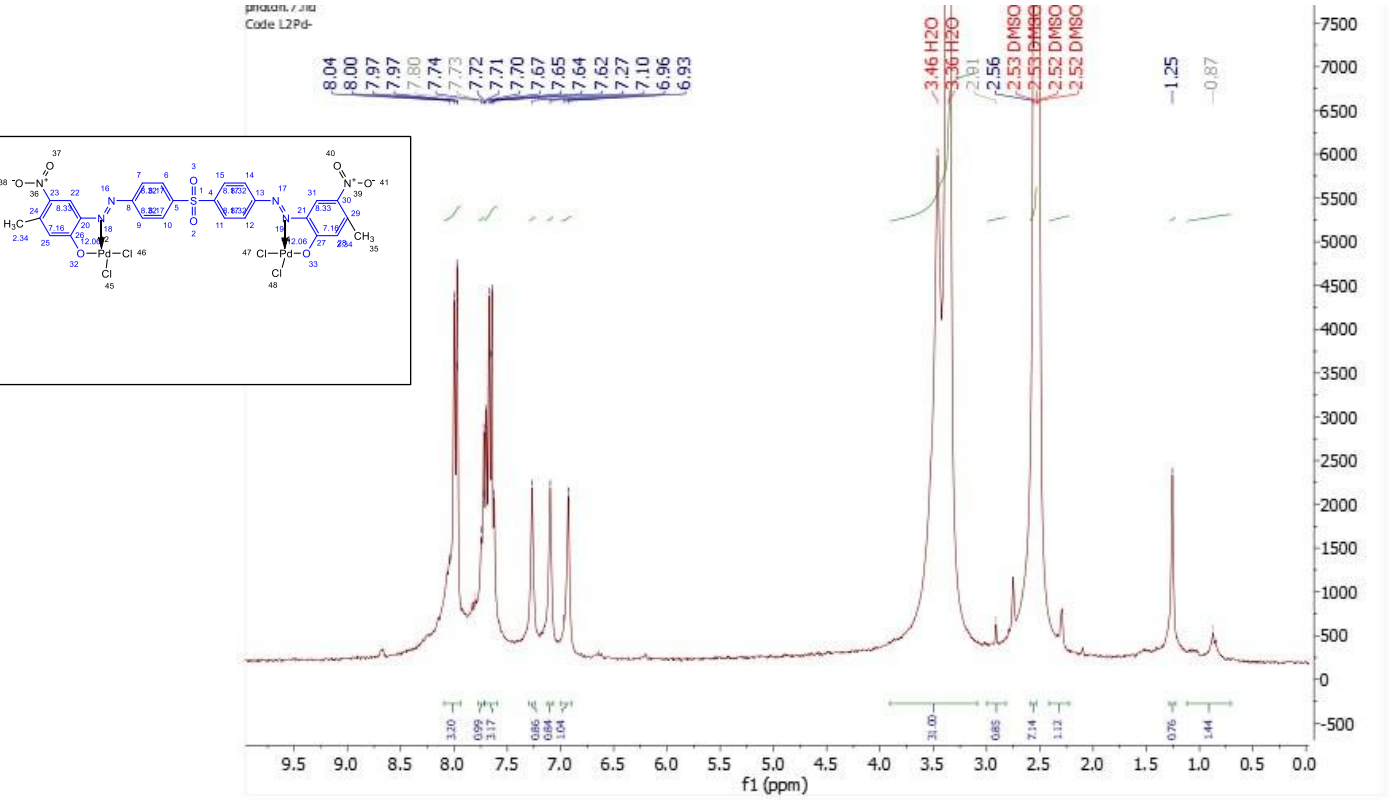

Figure 3 1HNMR spectrum of pd(II)Complex for SPD-DMN ligand in DMSO d6 solvent

Infrared spectra

Using KBr discs as the medium, infrared spectra of the SPD-DMN ligand and its Pd(II) complex were carefully obtained. In our analysis, the Fourier-transform infrared (FT-IR) spectrum revealed characteristic absorption bands of great importance. The free Bisazo Ligand and its Pd(II) Complex showed clear lines at 1505 cm^-1 (strong) and 1499 cm^-1 (weak) in the FT-IR spectra, respectively. The azo group (-N=N-) was definitively identified as the source of these bands (13). Surprisingly, differences appeared in the strength and location of these bands, offering strong proof of coordination processes involving this functional group. (14) .

Moreover, we identified faint bands associated with (M-N) vibrations at 509 cm^-1 in the complexes (15). A comprehensive compilation of the spectral data for both the ligand and its corresponding complexes is thoughtfully presented in Table 2 for reference and analysis.

Table 2 The important vibrations of SBDP-BN ligand and it Ag(I)complex

Group	□ (OH)	□ (C-H)	□ (C=C)	□ (N=N)	□ (S=O)	□ (C-O)	□ (C-N)	□ (M-O)	□ (M-N)
SPD-DMN	3430	1625	1402	1308	1154	1105	590	…….	…….
pd(II)	3432	3053	1155	1499	1630	1202	1155	669	509

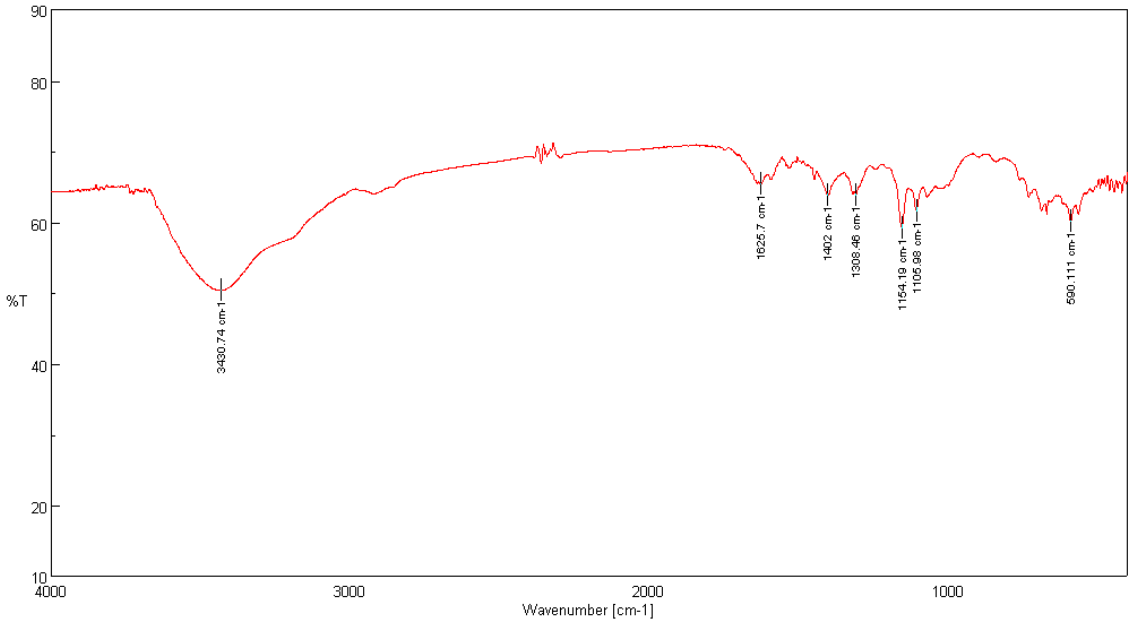

Figure 4 Infrared spectrum of SPD-DMN ligand

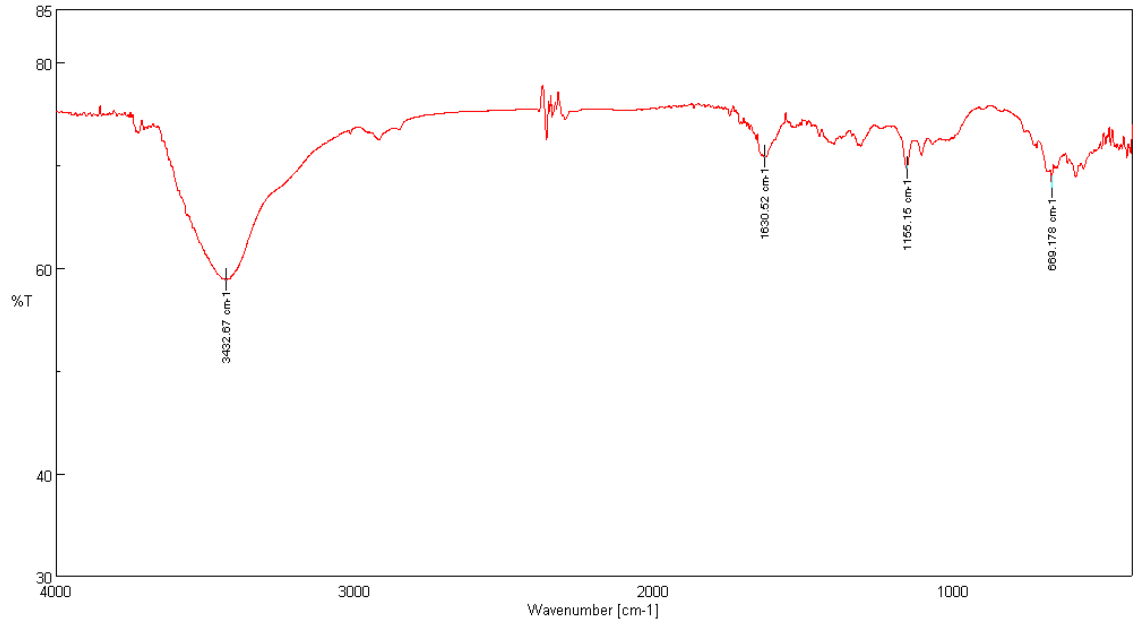

Figure 5 Infrared spectrum of pd(II)complex for SPD-DMN ligand

UV–Vis spectra of (SPD-DMN) ligand and pd (II) complex

Electronic transition measurements were conducted at room temperature in ethanol. In the ligand's spectrum, three prominent peaks were discerned: the first peak at 348.5 nm(equivalent to 28.0 69cm^-1), signifying the n → π* transition; the second peak at 269.5 nm(corresponding to 37.105 cm^-1), associated with the π → π* electron transition of the azo group (N=N); and notably, a third peak at 254 nm(equivalent to 39.370 cm^-1), indicating the (π → π*) electronic transition within the ethylenic moiety (C=C) of the aromatic ring. Meanwhile, the palladium complex displayed three distinct spectral peaks: the first two at 293 nm(equivalent to 34.129 cm^-1) and 266,5 nm(corresponding to 37.523 cm^-1) were attributed to charge transfer transitions (M→L, CT), while the third peak at 254.5 nm(equivalent to 39.292 cm^-1) represented internal transitions within the ligand itself.

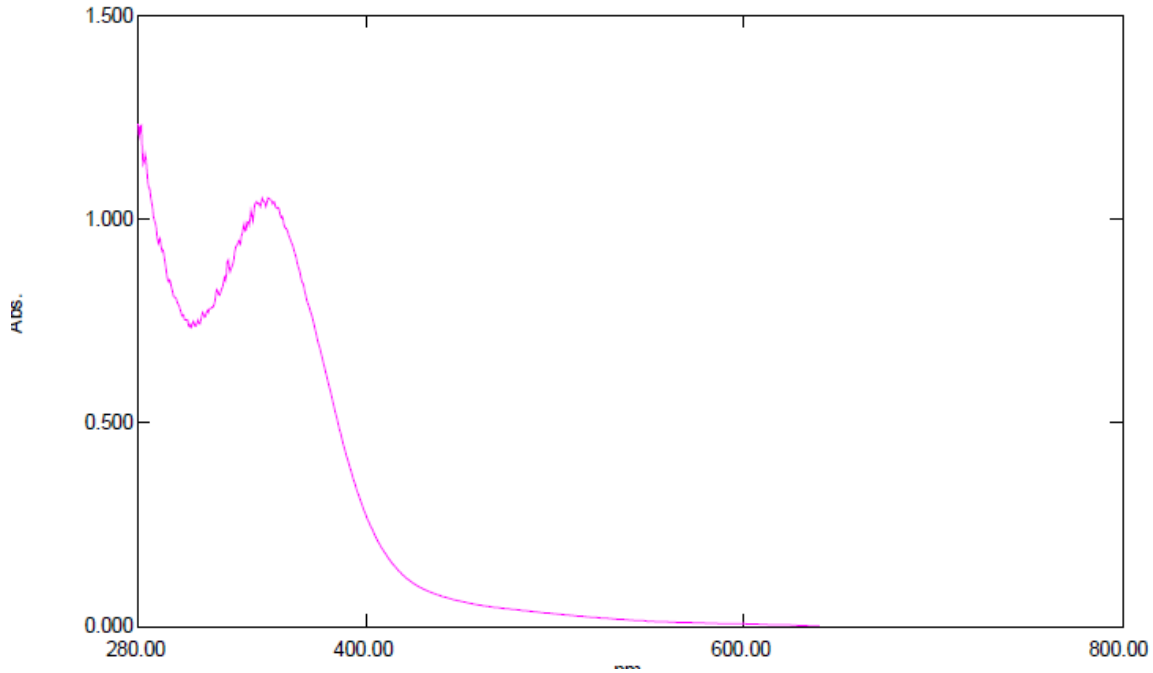

Figure 6 UV-Visible spectra of SPD-DMN ligand

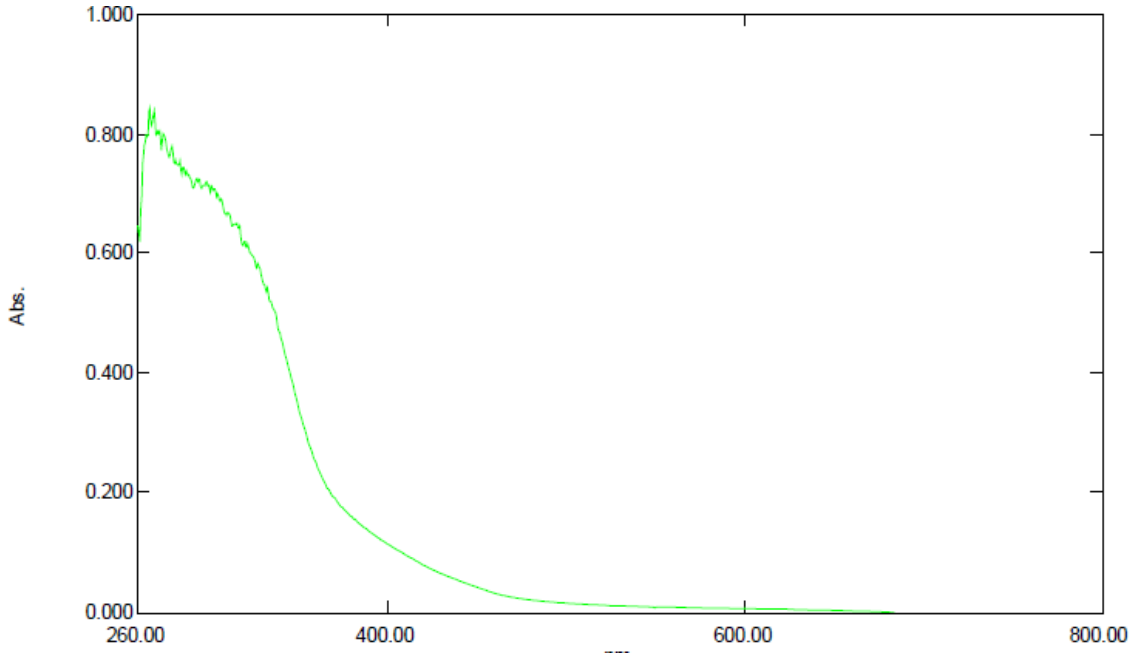

Figure 7 UV-Visible spectra of pd(II)complex

X-ray diffraction

The material was subjected to X-ray diffraction analysis using a lab X-ray diffractometer (Xrd). The acquired data showed that the angle at which X-rays deflect when they interact with the material is represented by two different peaks that are spread along this axis. Excel was used as the specialist data processing software for a thorough analysis in order to get quantitative insights from the data. The research revealed that these compounds exhibited nanoscale properties, with the ligand measuring an average of 18.02 nanometers and the pd(II) complex measuring an average of 28.71 nanometers. This is an important finding. These results highlight the compounds' nanostructured characteristics (16, 17), underscoring their potential application in a variety of scientific and technical fields that capitalize on the unique characteristics of nanomaterials.

Table 3 XRD Analysis Parameters for SBDP-BN and Ag(I) Complex

Compound	Pos. [−2Th.]	FWHM Left [−2Th.]	d-spacing [ŧ]	Height [cts]	Rel. Int. [%]	Crystallite Size(nm)	avg D(nm)	Lattice Strain
SPD-DMN	36.515	0.198	2.4587	1295	100	44.15	52.41	0.0026
	31.709	0.126	2.8196	8350	64.48	68.49		0.0019
	36.608	0.198	2.4587	6480	50.00	44.160		0.0026
pd(II)	22.180	0.1476	4.0079	679.3	100	57.31	56.86	0.0033
	12.144	0.1476	7.2882	244.2	35.95	56.56		0.0061
	14.803	0.1476	5.9842	204.4	30.10	56.71		0.0050

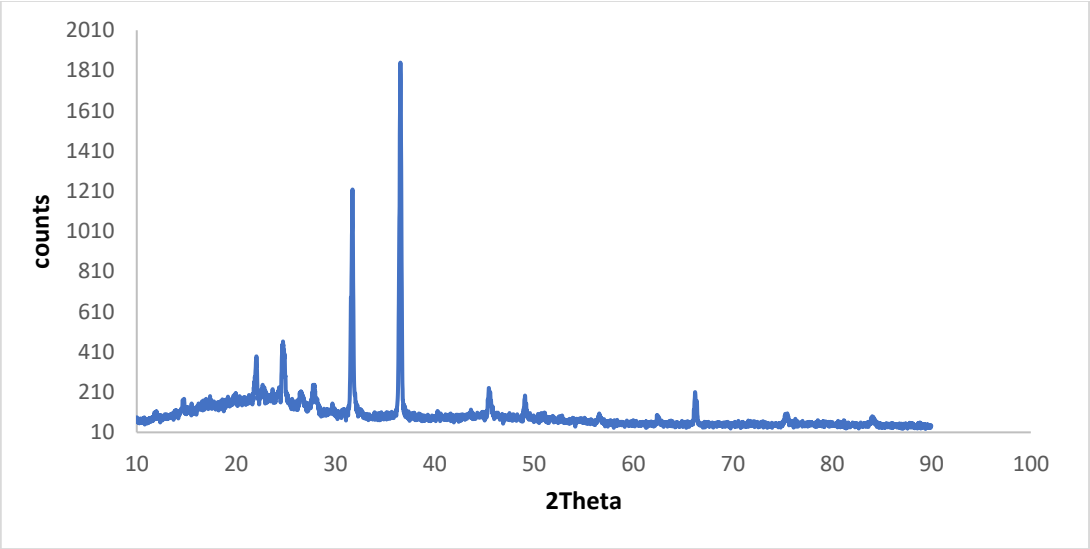

Figure 1 X-ray diffraction of *SPD-DMN* ligand

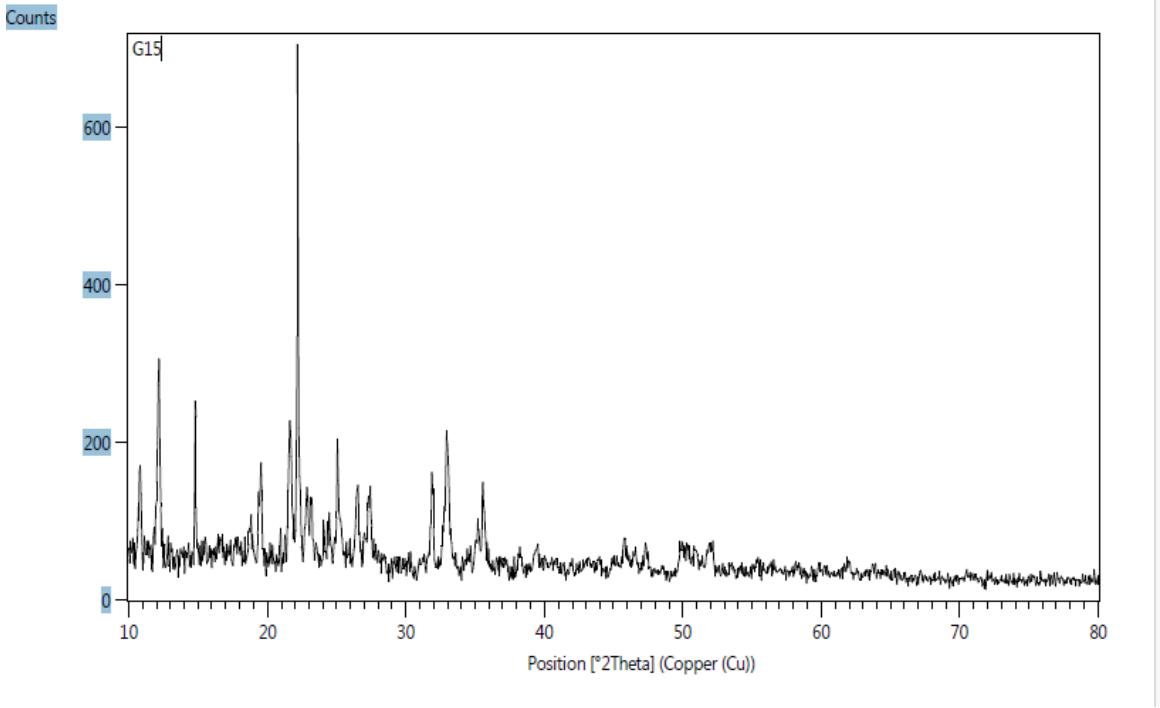

Figure 2 X-ray diffraction of pd(II)complex

Thermal Analysis of pd(II) Complex

Thermal analysis of the pd(II) complex involved a comprehensive investigation of its degradation behavior using thermogravimetric (TG) analysis. This analysis was carried out within a nitrogen atmosphere with a flow rate of 20 mL/min, spanning a temperature range from 20 to 700°C, and employing a heating rate of 20°C/min. The ensuing thermal stability findings are meticulously summarized in Table 3, and a representative Thermogravimetric Analysis (TGA) and Differential Thermogravimetry (DTG) diagram is thoughtfully depicted in Figure 13. The thermogravimetric analysis revealed a multi-step decomposition process, as evidenced by distinct peaks in the TGA and DTG data, characterized by varying Tmax values. These findings contribute essential insights into the thermal behavior and stability of the pd(II) complex

Table 4Thermal analyses data for (TGA,DTG,) of pd(II)Complex

Compound	Decomposition	TG Range (°C)	% Mass loss	% Total mass loss	DTA(°C) T_{max}	Metallic Residue
pd(II)-Complex	1st	205- 330.32	10.95		212.51	1/2pd_2O
	2nd	360.9-509.14	19.7	30.65	350.91	
	Residue	>642.85				

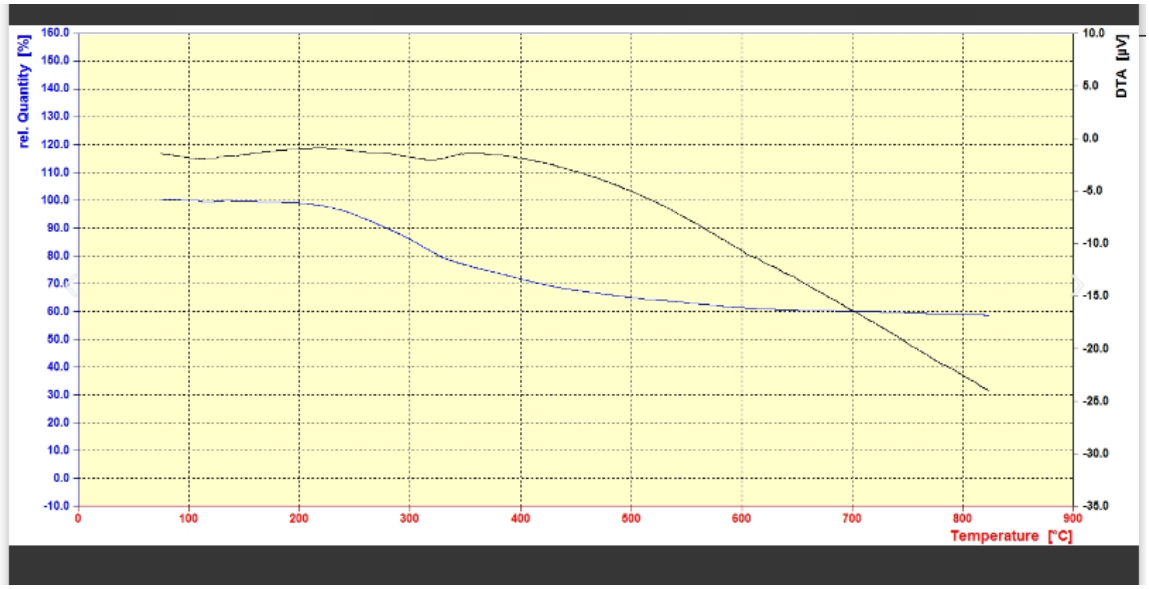

Figure 3 TGA-DTG- Curves of pd(II) Complex

Molecular Geometry for the SPD-DMN Ligand and Its PD(II) Complex

Avogadro, a flexible tool for manipulating and visualizing chemical compounds, was used to determine the molecular geometry of the SPD-DMN ligand and its corresponding pd(II) complex(18). The Universal Force Field (UFF) method(19), (20), a molecular

mechanics-based strategy targeted at decreasing potential energy to create the most energetically stable conformation, was utilized to optimize the molecular geometry. The molecular geometries that are most stable are depicted in Figures 14 and 15. The process of characterization involved a number of diagnostic measurements, such as molar ratios, magnetic studies, and evaluations of molar electrical conductivity. It also involved the use of several analytical techniques, including mass spectrometry, 1H-NMR, 13C-NMR, UV-visible spectroscopy, infrared spectroscopy, and thermal analysis. All together, these analyses offered insightful information about the SPD-DMN ligand's coordination behavior.

The results show that the SPD-DMN

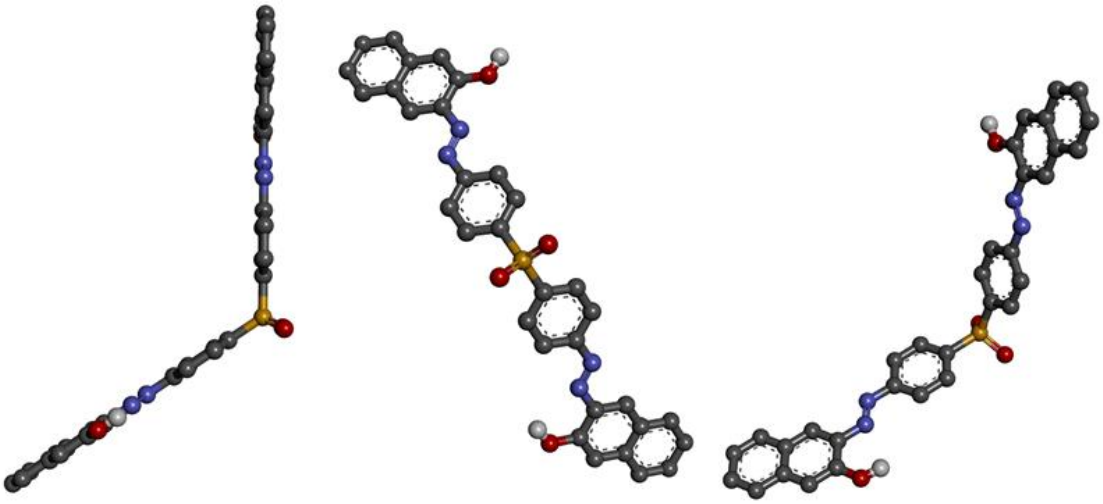

Figure 4 The lowest energy molecular geometry for ligand SPD-DMN.

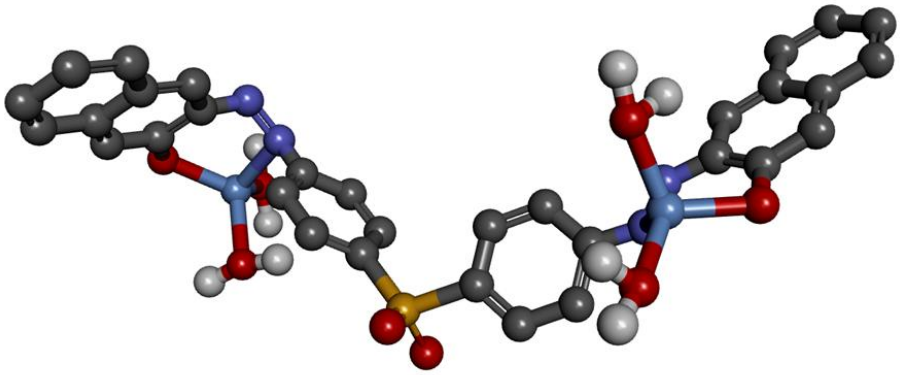

Figure 5 The lowest energy molecular geometry for a palladium complex.

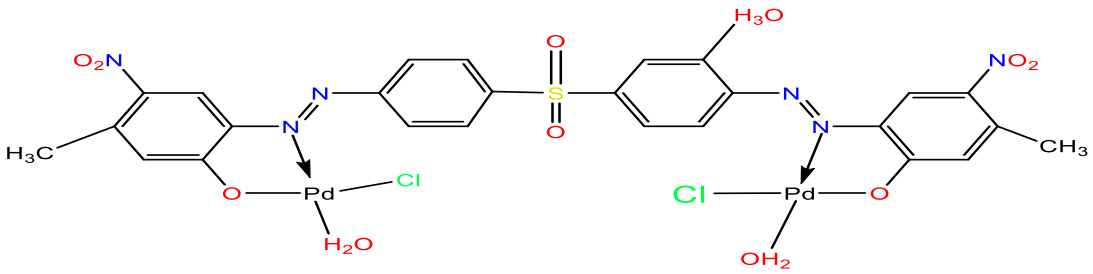

Figure 6 The proposed structural formula for the palladium (II) complex with ligand SPD-DMN.

Effects of Ligand SPD-DMN AND Its complex on Breast Cancer and Normal Cells

This investigation delves into the potential therapeutic efficacy of Ligand SPD-DMN against Breast cancer, specifically targeting HEPG2 cells. The MTT assay was employed to assess cell viability, revealing a concentration-dependent effect on cell survival, represented as the percentage of remaining viable cells(21). Remarkably, Breast cancer cells exhibited a range of remaining viability spanning from 18.33% to 85.66%, the Ligand SPD-DMN demonstrated a notably lower impact on HEPG2 cells at a concentration of 6.25 µg/ml, with the most substantial reduction in viability observed at 400 µg/ml for both cell lines. Notably, at 400 µg/ml, the Ligand SPD-DMN exhibited an impressive 14.33% reduction in viability for HEPG2 cells,. The IC50 values for the ligand were determined to be 75.59 µg/mL for liver cancer cells (HEPG2) and 97.31 µg/mL for normal cells Interpreting these values indicates the precise amount of the compound needed to inhibit cell growth by 50%(22).

The study reveals that the effect of the ligand on cancer cells and its effect on normal cells is nearly identical, indicating a lack of selectivity. To enhance its potential as a therapeutic agent, further research is needed to develop greater selectivity, ensuring that the ligand primarily targets cancer cells while minimizing its impact on normal cells. This improved selectivity is crucial for optimizing the ligand's efficacy and reducing potential side effects, ultimately making it a more promising candidate for cancer treatment.

Table 5 the effect of theligand and Its complex on the growth of breast cancer cells (HEPG2) In different concentrations.

Cons. (Mg/ml)	SPD.DMN		pd (II)	
	Mean %	Std error	Mean %	Std error
0	100	2.218342	100	2.218342
20	95.6881	1.660575	79.78457	0.663565
40	88.30547	3.415014	72.66559	1.312606
80	75.07717	1.160567	60.69775	2.368758
160	62.86817	2.710153	47.64309	2.573032
320	44.13826	1.519173	35.74598	4.422062
IC_{50} (Mg/ml)	254.4		143.4	

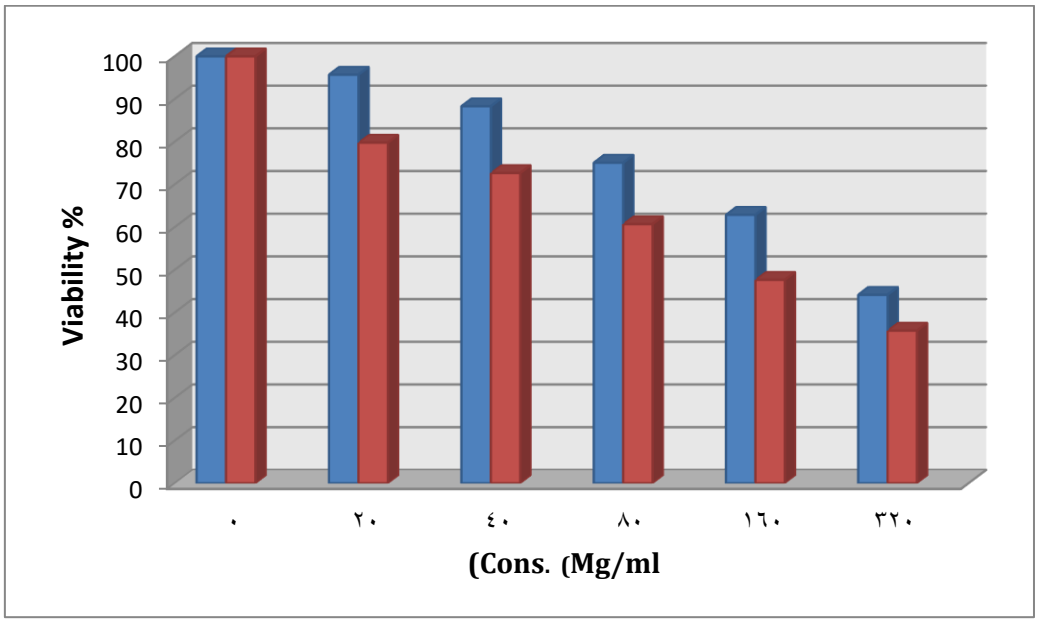

Figure 7 Comparing the impact of theligand and pd(II) complex on the proliferation of Breast cancer cells (HEPG2) at various concentrations.

Antioxidant Activity

results of an antioxidant test, indicating the percentage of inhibition of DPPH radicals at various concentrations for SPD-DMN, the pd(II) complex, and ascorbic acid (vitamin C)(23). SPD-DMN demonstrates a concentration-dependent antioxidant effect, with inhibition percentages ranging from 24.18% to 39.49%. The pd(II) complex exhibits slightly stronger antioxidant activity than SPD-DMN, with inhibition percentages ranging from 28.84% to 49.62%. In contrast, ascorbic acid consistently displays the highest antioxidant activity, with inhibition percentages ranging from 27.03% to 91.53% across the tested concentrations. These results underscore the moderate antioxidant potential of SPD-DMN and the pd(II) complex, while highlighting the superior antioxidative efficacy of ascorbic acid, which could serve as a reference for future antioxidant studies and potential therapeutic applications. Further investigations may be needed to optimize the antioxidant properties of SPD-DMN and the pd(II) complex.

Table 6 Antioxidant Activity Comparison of SPD-DMN, pd(II)Complex, and Ascorbic Acid Using different concentrations

Compound	IC50	% inhibition				
		50 µg/ml	150 µg/ml	250 µg/ml	350µg/ml	450 µg/ml
SPD-DMN	2.3898	2.052	1.946	1.943	1.908	1.884
pd(II)	1.8267	1.697	1.562	1.543	1.484	1.405
Ascorbic acid	0.3777	1.059	0.101	0.101	0.1	0.1

CONCLUSION

In conclusion, this study has unveiled the synthesis, characterization, and multifaceted biological activities of the novel Dapsone-derived bisazo ligand, SPD-DMN and its pd(II) complex. SPD-DMN demonstrates remarkable solubility, structural versatility, and tetradentate coordination behavior, making it a compelling candidate for coordination chemistry applications. The formation of the pd(II) complex further

highlights its potential therapeutic relevance. Evaluations of SPD-DMN antioxidant activity reveal moderate potential, while its impact on breast cancer cells (HEPG2) underscores the need for enhanced selectivity in its anticancer properties. These findings contribute significantly to the fields of coordination chemistry and cancer therapeutics, offering insights into the development of innovative anticancer agents. Moving forward, further research is imperative to optimize the selectivity of SPD-DMN, ultimately realizing its potential to revolutionize cancer treatment and alleviate the global burden of this formidable disease. This research marks a vital step toward the creation of more effective and targeted anticancer therapies, bringing hope for improved patient outcomes worldwide.

REFERENCES

[1] P. Kaul, R. Kumar, M. P. Singh, and P. K. Garg, "Social taboos: a formidable challenge in cancer care," *BMJ Case Rep*, vol. 14, no. 1, p. e236095, Jan. 2021, doi: 10.1136/bcr-2020-236095.

[2] K. D. Mjos, "Coordination chemistry of antimicrobial and anticancer agents," 2015. [Online]. Available: https://open.library.ubc.ca/collections/24/items/1.0166659

[3] R. G. Kenny and C. J. Marmion, "Toward Multi-Targeted Platinum and Ruthenium Drugs—A New Paradigm in Cancer Drug Treatment Regimens?," *Chem Rev*, vol. 119, no. 2, pp. 1058–1137, Jan. 2019, doi: 10.1021/acs.chemrev.8b00271.

[4] N. P. E. Barry and P. J. Sadler, "100 years of metal coordination chemistry: from Alfred Werner to anticancer metallodrugs," *Pure and Applied Chemistry*, vol. 86, no. 12, pp. 1897–1910, Dec. 2014, doi: 10.1515/pac-2014-0504.

[5] N. Q. Shikhaliyev *et al.*, "Noncovalent interactions in the design of bis-azo dyes," *CrystEngComm*, vol. 21, no. 34, pp. 5032–5038, 2019, doi: 10.1039/C9CE00956F.

[6] P. P. T. Sah, "The antitubercular activity of azo dyes. I. Bisazo dyes derived from tetrazotized bis(4-aminophenyl)-sulfone and various coupling components," *Recueil des Travaux Chimiques des Pays-Bas*, vol. 69, no. 11, pp. 1407–1434, Sep. 2010, doi: 10.1002/recl.19500691110.

[7] A. B. Syeda, A. Banu syeda, M. Ferazoddin, M. Rajeswari, J. P. Paul, and B. Juluru, "Design, Synthesis and Anticancer Evaluation of Benzoxazole Resemble Substituted Arylamide Derivatives of Bis-1,3,4-Oxadiazole-oxazolo[4,5-b]pyridin-2-yl) as Anticancer Agents," *Chemical Data Collections*, vol. 43, p. 100971, Feb. 2023, doi: 10.1016/j.cdc.2022.100971.

[8] V. Pillai, R. Kadu, L. Buch, and V. K. Singh, "Derivatives of Dapsone (dap): Synthesis and Study on *In Vitro* Anticancer Activity and DNA Laddering Against Hep G2 and C6 Human Cancer Cell Lines," *ChemistrySelect*, vol. 2, no. 16, pp. 4382–4391, May 2017, doi: 10.1002/slct.201700701.

[9] G. Şeker Karatoprak, "Antioxidants with hepatoprotective activity," in *Influence of Nutrients, Bioactive Compounds, and Plant Extracts in Liver Diseases*, Elsevier, 2021, pp. 209–225. doi: 10.1016/B978-0-12-816488-4.00008-5.

[10] S. George and H. Abrahamse, "Redox Potential of Antioxidants in Cancer Progression and Prevention," *Antioxidants*, vol. 9, no. 11, p. 1156, Nov. 2020, doi: 10.3390/antiox9111156.

[11] D. C. Muddiman, "Jürgen H. Gross: Mass spectrometry: a textbook, 3rd ed.," *Anal Bioanal Chem*, vol. 410, no. 8, pp. 2051–2052, Mar. 2018, doi: 10.1007/s00216-018-0870-8.

[12] P. Ferranti and G. Picariello, "Mass Spectrometry: Applications," in *Encyclopedia of Food and Health*, Elsevier, 2016, pp. 654–660. doi: 10.1016/B978-0-12-384947-2.00448-7.

[13] S. K. Kyei, O. Akaranta, and G. Darko, "Synthesis, characterization and antimicrobial activity of peanut skin extract-azo-compounds," *Sci Afr*, vol. 8, p. e00406, Jul. 2020, doi: 10.1016/j.sciaf.2020.e00406.

[14] J. Wang, N.-N. Chen, C. Zhang, L.-Y. Jia, and L. Fan, "Functional group induced structural diversities and photocatalytic, magnetic and luminescence sensing properties of four cobalt(<scp>ii</scp>) coordination polymers based on 1,3,5-tris(2-methylimidazol-1-yl)benzene," *CrystEngComm*, vol. 22, no. 4, pp. 811–820, 2020, doi: 10.1039/C9CE01474H.

[15] T. Stüker, H. Beckers, and S. Riedel, "A Cornucopia of Iridium Nitrogen Compounds Produced from Laser-Ablated Iridium Atoms and Dinitrogen," *Chemistry – A European Journal*, vol. 26, no. 33, pp. 7384–7394, Jun. 2020, doi: 10.1002/chem.201905514.

[16] R. Bhatt and S. Gupta, "Nano Particles and Their Mode of Action in Environment," 2018, pp. 212–219. doi: 10.4018/978-1-5225-3126-5.ch013.

[17] C. J. Kuijpers, H. P. Huinink, N. Tomozeiu, S. J. F. Erich, and O. C. G. Adan, "Nano-particle dynamics during capillary suction," *J Colloid Interface Sci*, vol. 521, pp. 69–80, Jul. 2018, doi: 10.1016/j.jcis.2018.03.023.

[18] H. D. Snyder and T. G. Kucukkal, "Computational Chemistry Activities with Avogadro and ORCA," *J Chem Educ*, vol. 98, no. 4, pp. 1335–1341, Apr. 2021, doi: 10.1021/acs.jchemed.0c00959.

[19] L. Jaillet, S. Artemova, and S. Redon, "IM-UFF: Extending the universal force field for interactive molecular modeling," *J Mol Graph Model*, vol. 77, pp. 350–362, Oct. 2017, doi: 10.1016/j.jmgm.2017.08.023.

[20] A. Nagar, A. Garg, S. Singh, L. Gao, J. Kim, and K. Wei, "Reactive Force Field (ReaxFF) and Universal Force Field Molecular Dynamic Simulation of Solid Electrolyte Interphase Components in Lithium-Ion Batteries," *Journal of Electrochemical Energy Conversion and Storage*, vol. 21, no. 2, May 2024, doi: 10.1115/1.4062992.

[21] M. Ghasemi, T. Turnbull, S. Sebastian, and I. Kempson, "The MTT Assay: Utility, Limitations, Pitfalls, and Interpretation in Bulk and Single-Cell Analysis," *Int J Mol Sci*, vol. 22, no. 23, p. 12827, Nov. 2021, doi: 10.3390/ijms222312827.

[22] P. Liu, H. Xing, S. Cao, S. Fan, and T. Sun, "Study on IC50 prediction of targeted drugs for hepatoma cells based on SSA-BP neural network," in *International Conference on Cloud Computing, Performance Computing, and Deep Learning (CCPCDL 2022)*, S. Saxena, Ed., SPIE, Oct. 2022, p. 91. doi: 10.1117/12.2641052.

[23] G. Celiz, M. Renfige, and M. Finetti, "Spectral analysis allows using the DPPH* UV–Vis assay to estimate antioxidant activity of colored compounds," *Chemical Papers*, vol. 74, no. 9, pp. 3101–3109, Sep. 2020, doi: 10.1007/s11696-020-01110-8.